

Laboratory experiments and simulations on jets

Martín Huarte-Espinosa*, Adam Frank and Eric G. Blackman

Department of Physics and Astronomy, University of Rochester, 600 Wilson Boulevard, Rochester, NY, 14627-0171

Abstract

Astrophysical jets have been studied with observations, theoretical models and numerical simulations for decades. Recently, supersonic magnetized jets have been formed in laboratory experiments of high-energy density plasmas. I will review these studies and discuss the experimental setup that has been used to form millimeter-scale jets driven by strong toroidal magnetic fields in a MAGPIE generator. The physical conditions of these experiments are such that they can be scaled to astrophysical scenarios. These laboratory jets provide insights on the underlying physics of magnetic tower jets and help constrain some models of astrophysical jets. In this context, we also discuss the connection between the laboratory jets and recent 3D-MHD numerical simulations of Poynting flux dominated jets. The simulations allow us to investigate the effects of thermal energy losses and base rotation on the growth rate of kink mode perturbations, and to compare the evolution of PFD jets with a hydrodynamic counterpart of the same energy flux.

1 Introduction

Jets are observed in Young Stellar Objects, post-AGB stars, X-ray binaries, radio galaxies and other astrophysical objects. Models suggest that jets are launched and collimated inside their “central engine” by a symbiosis of accretion, rotation and magnetic mechanisms (Pudritz et al. 2007). The engines cannot be directly observed however, because telescopes have insufficient resolution. Recently, laboratory astrophysics experiments have provided scale models of the launch and propagation of magnetized jets with dimensionless parameters relevant for astrophysical systems (Lebedev et al. 2005; Ciardi et al. 2009; Suzuki-Vidal et al. 2010). These studies, when combined with numerical simulations (Ciardi et al. 2007; Huarte-Espinosa et al. 2011), can help to resolve unanswered questions in jet physics. A fundamental distinction can be made between the physics of jet launch and that of jet propagation far from the engine. Since we cannot resolve the former observationally, it is important to identify distinct features of jets in the asymptotic propagation regime that can distinguish different engine paradigms. While both simulations and experiments now consistently reveal the promise, if not essentiality, of dynamically significant magnetic fields for jet launch, the correlation between the initial jet magnetic configuration and the stability of the flow far from the launching region is unclear. The importance of the magnetic field relative to the flows’ kinetic energy divides jets into (i) Poynting flux dominated (PFD; Shibata & Uchida 1986), in which magnetic fields dominate the jet structure, (ii) magnetocentrifugal (Blandford &

*martinhe@pas.rochester.edu

Payne 1982), in which magnetic fields only dominate out to the Alfvén radius. The observable differences between PFD and magnetocentrifugal jets are unclear, as are the effects that cooling and rotation have on PFD jets.

2 Laboratory experiments

Experiments and numerical modelling of astrophysically relevant supersonic plasma jets have been performed by a number of authors using high intensity lasers (see e.g. Farley et al. 1999; Shigemori et al. 2000; Foster et al. 2002; see also review in Blackman 2007). In this section however, we focus on magnetized jet experiments which have dimensionless numbers (Reynolds, magnetic Reynolds and Peclet) in reasonably appropriate regimes for astrophysics and have used conical wire arrays and conducting foils on pulsed power facilities (Lebedev et al. 2005; Ciardi et al. 2007,2009; Suzuki-Videl et al. 2010).

2.1 Wire array, toroidal field

Lebedev et al. (2005) applied a TW electrical pulse (1 MA, 250 ns) to an array of wires located inside a vacuum chamber. The set up consisted of a pair of concentric electrodes connected radially by tungsten wires of $13\ \mu\text{m}$ in diameter. The current causes ablation of the wires which results in the formation of a background ambient plasma (Fig. 1a). This material is then pushed above the wires by Lorentz forces, and resistive diffusion keeps the current close to the wires. The current induces a toroidal magnetic field which at this stage is confined below the wires, around the central electrode. Then, after the complete ablation of the wires near the central electrode, the current switches to the plasma and creates a magnetic cavity (Fig. 1b) with a jet at its center. The core of the jet is confined and accelerated upward by the pressure of the toroidal field. The return current flows along the walls of the magnetic cavity, which is in turn confined by both the thermal pressure and the inertia of the ambient plasma. Next, the magnetic cavity opens up, the jet becomes detached and it propagates away from the source at a velocity of order $200\ \text{km s}^{-1}$ (Fig. 1c).

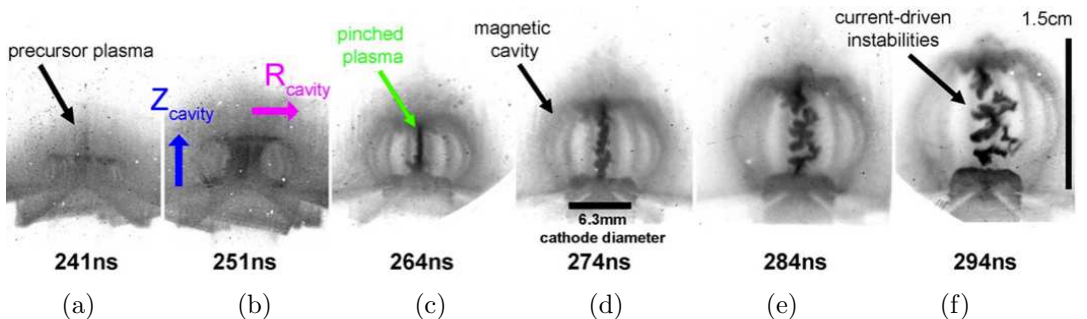


Figure 1: Time sequence of soft X-rays images showing the formation of the background plasma (a), the expansion of the magnetic cavity (b), the launch of the jet (c), the development of instabilities in the central jet column (d) and the fragmentation of the jet (e,f). The wire array shows in the bottom part of the figures. Image taken from Suzuki-Vidal et al. (2010).

Finally, instabilities, which resemble those of the kink mode ($m = 1$), develop within the body of the jet (Fig. 1d). The outflow is then fragmented into well collimated structures with characteristic axial non-uniformities (Fig. 1e,f; Lebedev et al. 2005). We note that a critical ingredient of these experiments is the significant thermal energy loss of both the jet and the

ambient plasmas. This is relevant because cooling plays a critical role in many astrophysical jet environments, e.g. YSOs.

The experiment was reproduced a few years later by Ciardi et al. (2007) using 3-D non-ideal MHD simulations. A numerical model was carefully designed to simulate the laboratory components (electrodes and wires) and all the plasma evolution phases. Good agreement was found between the simulations and the experiments (Ciardi et al. 2007). The simulations showed that during the final unstable phase of jet propagation, the magnetic fields in the central jet adopted a twisted helical structure. This confirmed that the jets are affected by normal mode, $m = 1$, perturbations.

2.2 Wire array, toroidal and axial fields

A subsequent series of experiments were carried out by Suzuki-Vidal et al. (2010) who studied the effect of introducing an axial magnetic field, B_z , into a radial wire array. Their experimental configuration was the same as that of Lebedev et al. (2005, above), but they placed two solenoids below the wires, into the path of the current. Suzuki-Vidal et al. (2010) found that the added B_z affects the degree of compression of the on-axis pinch of the jet. As they increased the magnitude of B_z , the plasma column radially expanded after reaching a minimum radius. They also saw that jets are more stable when B_z is present than otherwise. We note that this stability effect can be explained analytically (with perturbation theory on a plasma column) and numerically (section 3) as a result of magnetic pressure from B_z acting against hoop stress compression from the toroidal field component.

2.3 Conducting foil

Ciardi et al. (2009) extended the experiments of Lebedev et al. (2005) by replacing the wire array (section 2.1) by a $6 \mu\text{m}$ thick aluminum foil. Ciardi et al. (2009) found the following. The conducting foil experiment produced very similar results than the wire array one. However, while the wire array experiment results in the launch of one jet only, the conducting foil experiment results in a series of jets which are launched sequentially (Fig. 2). The plasma flux caused by ablation of the foil is much larger than that of the wires; the foil provides an increased mass as a function of radius. Thus the current gap produced by the magnetic cavity (section 2.1) is smaller in the foil experiment than in the wire array one, and can be refilled by the readily available plasma. Closure of the gap, which does not happen in the wire array case, allows the current to flow once again across the base of the magnetic cavity, thus re-establishing the initial configuration. Once the magnetic pressure is large enough to break through this newly deposited mass, a new jet/bubble ejection cycle begins (Ciardi et al. 2009). This constituted the first laboratory study to address time-dependent episodic jet launch.

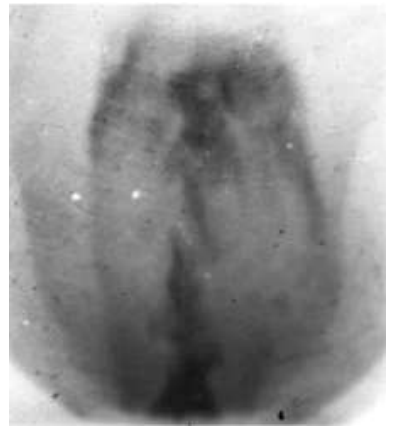


Figure 2: Filtered XUV emission images of one of the episodic jet experiments. The clumpy jet at the center is contained inside three nested magnetic bubbles which were formed by previously launched jets (Ciardi et al. 2009).

3 Simulations

3.1 Model

We use the Adaptive Mesh Refinement code AstroBEAR2.0 (Cunningham et al. 2009; Carroll-Nellenback et al. 2011) to solve the equations of radiative-MHD in 3D. The grid represents $160 \times 160 \times 400$ AU divided into $64 \times 64 \times 80$ cells plus 2 adaptive refinement levels. We use periodic boundary conditions at the four vertical faces of the domain, extrapolation conditions at the top face and a combination of reflective and inflow conditions at the bottom face. Initially, molecular gas is static and has an ideal gas equation of state ($\gamma = 5/3$), a number density of 100 cm^{-3} and a temperature of 10000 K. The magnetic field is helical, centrally localized and given by the vector potential (in cylindrical coordinates)

$$\mathbf{A}(r, z) = \begin{cases} \frac{r}{4}(\cos(2r) + 1)(\cos(2z) + 1)\hat{\phi} + \frac{\alpha}{8}(\cos(2r) + 1)(\cos(2z) + 1)\hat{k}, & \text{for } r, z < r_e; \\ 0, & \text{for } r, z \geq r_e, \end{cases} \quad (1)$$

where $r_e = 30$ AU and $\alpha = 40$ has units of length and determines the ratio of toroidal to poloidal magnetic fluxes. The magnetic pressure exceeds the thermal pressure inside the magnetized region.

Source terms continually inject magnetic or kinetic energy at cells $r, z < r_e$. We carry out 4 simulations: an adiabatic, a cooling, a rotating PFD jet, and a hydrodynamical jet. The latter is constructed to have same time average propagation speed and energy flux as the adiabatic PFD jet. The cooling tables of Dalgarno & McCray (1972) were used for the cooling case. For the rotating case we allowed the gas and magnetic fields within $r, z < r_e$ to move in Keplerian rotation.

3.2 Results

Magnetic pressure pushes field lines and plasma upward, forming magnetic cavities with low density (Fig. 3, all but right panel). The adiabatic case is the most stable. PFD jets decelerate more quickly relative to our hydro jet. This results because the PFD and hydro jets have the same injected energy flux, but the PFD case produces not only axial but radial expansion. The pre-collimated hydro can only expand via a much lower thermal pressure. Thus all of the energy flux in the hydro case for our set up is more efficiently directed to axial mechanical power. In principle, our hydro case can emulate

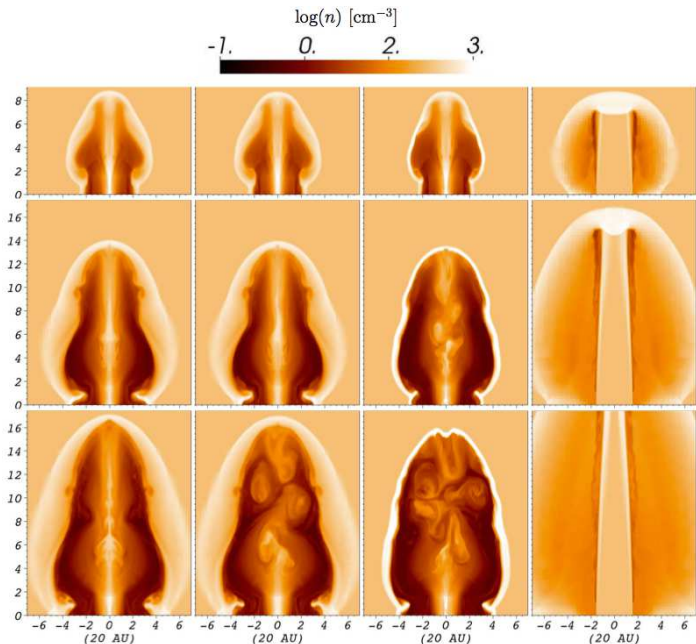


Figure 3: Logarithmic density maps of the adiabatic (1st column), rotating (2nd column) and cooling (3rd column) PFD jets. Hydrodynamic jet (4th column). From top to bottom the time is 42, 84 and 118yr.

the asymptotic propagation regime of a jet that was magneto-centrifugally launched (e.g. Blackman 2007) which is distinct from a PFD jet.

The PFD jet cores are thin and unstable, whereas the hydro jet beam is thicker, smoother and stable. The PFD jets are sub-Alfvénic. Their cores are confined by magnetic hoop stress, while their surrounding cavities are collimated by external thermal pressure. PFD jets carry high axial currents which return along their outer contact discontinuity.

We see that the inner regions of the PFD jets, just outside the core, are low beta plasma columns in which the axial magnetic field dominates over the toroidal one, $|B_\phi/B_z| \ll 1$. The columns' instability condition is given by

$$\left| \frac{B_\phi}{B_z} \right| > |(\beta_z - 1)kr_{jet}|, \quad (2)$$

where $\beta_z = 2\mu_0 P/B_z^2$, μ_0 is the magnetic vacuum permeability, P is the plasma thermal pressure and k^{-1} is the characteristic wavelength of the current-driven perturbations. We find that the cooling jet shows $\beta_z \sim 1$ from early in the simulation (Fig. 4), and thus does not have sufficient thermal energy to damp the magnetic pressure kink perturbations. The latter grow exponentially.

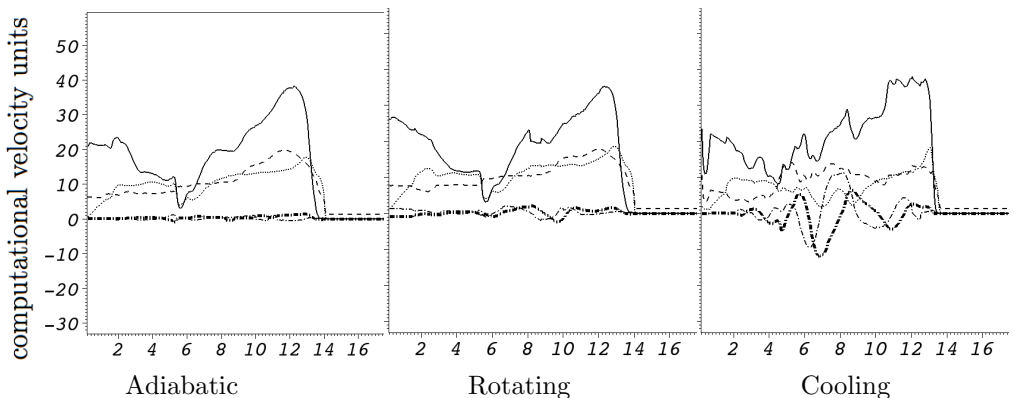


Figure 4: Plasma velocities along the axes of the PFD jets after expanding for 84 yr. The solid, dashed, dotted, dot-dash and dot-dash thick lines represent the Alfvén speed, the sound speed, v_z , v_x and v_y , respectively. Each velocity unit represents 9.1 km s^{-1} .

A different path to instability operates for the rotating (non-cooling) case. For this case, rotation at the base of the jet causes a slow amplification of the toroidal magnetic field. Hence the left hand side of equation (2) increases slowly, and so do the kink mode perturbations. The rotating jet is not completely destroyed by these perturbations, and their amplitude is about twice the radius of the central jet (Fig 5), in agreement with the Kruskal-Shafranov criterion (Kruskal et al. 1958; Shafranov 1958).

In Figure 4 we show profiles of the relevant velocities of the PFD jets along the jet axis, as a function of cooling and rotation. We also followed these in time. During the stable propagation phase, we find that the jets are mostly sub-Alfvénic and trans-sonic, independent of cooling or rotation. Fast-forward compressive MHD (FF) and transmitted hydrodynamic shocks are evident in the ambient medium, ahead of the jets. The FF shocks steepen in time,

whereas the hydrodynamic shocks are quickly dissipated in the cooling case. In contrast, the adiabatic and rotating cases show regions within the lower half of the jets, where the sound speed is super-Alfvénic. Such regions are bounded by the reverse and the forward slow-modes of compressive MHD waves, and characterized by high thermal to magnetic pressure ratios.

4 Conclusions

PFD jets can be produced in pulsed power laboratory facilities and help to understand the physics of astrophysical jets. The PFD “lab jets” are collimated by hoop stress, and their outer magnetic cavities are collimated by external pressure. The axial magnetic component influences both the radial compression and the stability of the jets. The outflows evolve to become corrugated, but still collimated, structures due to current-driven instabilities. Thin conduction foil experiments produce episodic jets and nested magnetic bubbles. Observations of multiple lobes in the radio galaxy B0925+420, may be consistent with such processes (Brocksopp et al. 2007).

Our simulations show that PFD jet beams are

lighter, slower and less stable than pre-collimated asymptotically hydrodynamic jets. In practice the latter could represent the asymptotic propagation regimes of magneto-centrifugally launched jets, which are distinct from PFD in that PFD remain PFD out to much larger scales. We find that current-driven perturbations in PFD jets are amplified by both cooling and rotation for the regimes studied: Shocks and thermal pressure support are weakened by cooling, making the jets more susceptible to kinking. Rotation amplifies the toroidal magnetic field which also exacerbates the kink instability. Our simulations agree well with the models and experiments of Shibata & Uchida (1986) and Lebedev et al. (2005), respectively.

Acknowledgements. Financial support for this project was provided by the Space Telescope Science Institute grants HST-AR-11251.01-A and HST-AR-12128.01-A; by the National Science Foundation under award AST-0807363; by the Department of Energy under award de-sc0001063; by NSF grant PHY0903797, and by Cornell University grant 41843-7012.

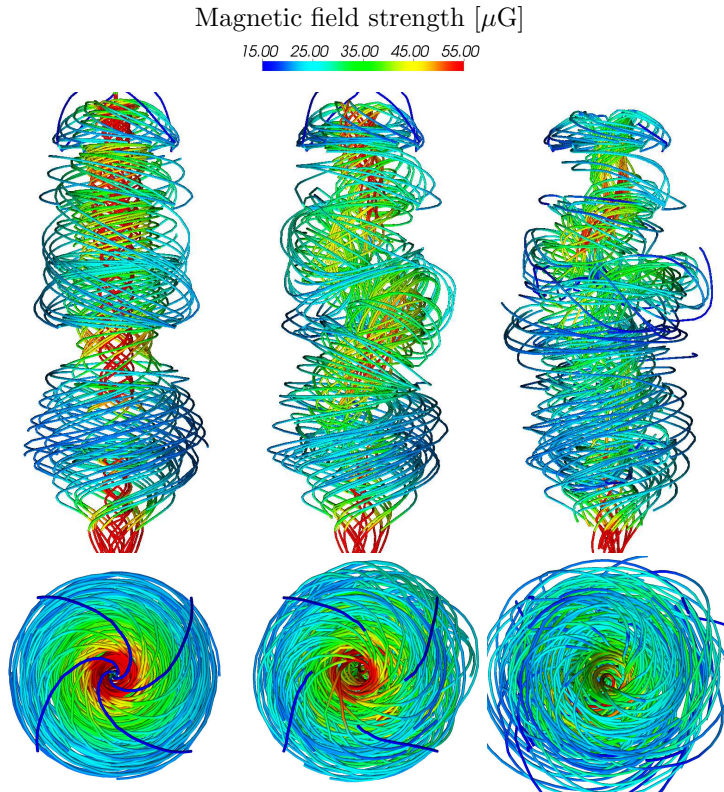


Figure 5: Central magnetic field lines at $t = 118$ yr. From left to right these are the adiabatic, the rotating and the cooling PFD jets, respectively. Bottom panels show a pole-on view.

References

- Blackman E.G., 2007, *Ap&SS*, 307, 7
- Blandford, R. D., & Payne, D. G., 1982, *MNRAS*, 199, 883
- Brocksoopp, C., Kaiser, C. R., Schoenmakers, A. P., & de Bruyn, A. G., 2007, *MNRAS*, 382, 1019
- Carroll-Nellenback, J.J., Frank, A., Shroyer, B., & Ding, C., 2011 (in prep)
- Ciardi, A., Lebedev, S. V., Frank, A., et al., 2007, *Physics of Plasmas*, 14, 056501
- Ciardi, A., Lebedev, S. V., Frank, A., et al., 2009, *ApJL*, 691, L147
- Cunningham A. J. et al., 2009, *ApJS*, 182, 519
- Dalgarno A., McCray R. A., 1972, *ARA&A*, 10, 375
- Farley, D. R., Estabrook, K. G., Glendinning, S. G., et al., 1999, *Physical Review Letters*, 83, 1982
- Foster, J. M., Wilde, B. H., Rosen, P. A., et al., 2002, *Physics of Plasmas*, 9, 2251
- Huarte-Espinosa, M., Frank A., Blackman E. G., Lebedev S., Ciardi A., Hartigan, P., 2011, *ApJ*, (in prep)
- Kruskal, M. D., Johnson, J. L., Gottlieb, M. B., Goldman, L. M., 1958, *Physics of Fluids*, 1, 421
- Lebedev, S. V., et al., 2005, *MNRAS*, 361, 97
- Pudritz, R. E., et al., 2007, *Protostars and Planets V*, 277
- Nakamura, M., & Meier, D. L., 2004, *ApJ*, 617, 123
- Shafranov, V. D., 1958, *Soviet Journal of Experimental and Theoretical Physics*, 6, 545
- Shibata, K., & Uchida, Y., 1986, *PASJ*, 38, 631
- Shigemori, K., Kodama, R., Farley, D. R., et al., 2000, *PRE*, 62, 8838
- Suzuki-Vidal, F., Lebedev, S. V., Bland, S. N., et al., 2010, *IEEE Transactions on Plasma Science*, 38, 581